ACCURACY ASSESSMENT OF DIGITAL SURFACE MODEL AND ORTHOPHOTO DERIVED FROM UAV PHOTOGRAMMETRY

Shofiyatul Qoyimah[1] and Yi-Hsing Tseng[1]
[1]National Cheng Kung University (NCKU), University Road No. 1, Tainan City 701, Taiwan (R.O.C),
Email: shofiyatulqoyimah@gmail.com
[1]National Cheng Kung University (NCKU), University Road No. 1, Tainan City 701, Taiwan (R.O.C),
Email: tseng@mail.ncku.edu.tw

KEY WORDS: Aerial triangulation, Check point, RMSE

ABSTRACT: Unmanned Aerial Vehicle (UAV) Photogrammetry that provides meter to centimeter measurement accuracy can fill the gap between conventional airborne and very-high-resolution satellite imagery in mapping application. The availability of Digital Surface Model (DSM) and orthophoto at high spatial and temporal resolution and accuracy is important for all activities that require accurate topographic data sets. Accuracy assessment of DSM and orthophoto derived from UAV photogrammetry technique has been chosen as a main goal on this study. For this study, three data sets were carried out considering three flight altitudes (i.e., 200, 400 and 600 m). For each dataset, aerial images were acquired in north-south and east-west direction block. Three aerial triangulation different test sets were conducted based on georeferencing technique, used Real Time Kinematic (RTK) followed by Post Processing Kinematic (PPK) process only, control point (5GCP) only and its combination (RTK/PPK+5GCP). The UAV was a fixed-wing platform named eBee Plus SenseFly and the sensor was Sensor Optimized for Drone Application (S.O.D.A) camera by SenseFly company. Pix4Dmapper software were used to process aerial triangulation followed by DSM and orthophoto generation using 5 Ground Control Points and 27 check points. Check points ground coordinate accuracy were calculated using Root Mean Square Error which compared their coordinate calculated from aerial triangulation process, digitized from DSM and orthophoto through measured from geodetic survey. The best accuracy in horizontal and vertical direction can be achieved by flying UAV at 200 m altitude using any georeferencing technique except in vertical direction while use GCP only. Check point accuracy from DSM and orthophoto digitizing was worse than from aerial triangulation process. Due to the influence of aerial triangulation result, more careful experiment and analysis on it was mandatory conducted to see the possibility of using UAV photogrammetry as alternative measurement technique in the future.

1. INTRODUCTION

1.1 Motivation and Aim

Recently, Unmanned Aerial Vehicle (UAV) is commonly used in Photogrammetry and Remote Sensing communities. UAV is the vehicle that remotely controlled, semi-autonomous, autonomous or a combination of these types. A digital camera as a measurement system in photogrammetry, can be equipped on the UAV to do a photogrammetric measurement work. This description then can be understood as an UAV photogrammetry.

Compared with other measurement method such as aerial and close range photogrammetry, UAV photogrammetry has supremacy features especially in project planning and its application. When the other methods only can be served in semi-automatic or manual project planning, UAV Photogrammetry can be planned in both automatically and manually. UAV Photogrammetry can be applied in small and large-scale areas including archaeological documentation, monitoring of hazards, 3D modelling of building and object in real-time measurement. The main advantage of using UAV Photogrammetry is its capability to be used in high risk situation, inaccessible areas and at the low altitude where manned system cannot be flown.

In mapping application, many measurement methods like interferometry, surveying, Ground Positioning System (GPS) and remote sensing provide different level of accuracy from micron to meter rely on its object or area size from submeter to kilometer. UAV Photogrammetry can cover area from meter to kilometer size which centimeter to meter level of accuracy can be achieved. Based on this reason, the main goal of this study is the assessment of UAV photogrammetry measurement accuracy by analysing the aerial triangulation and DSM and orthophoto generation result.

1.2 Previous Work

Accuracy assessment in previous work is more talked about aerial triangulation result including GCP and check point positioning error and also DSM and orthophoto generation result. (Kim et al. 2013) propossed a new technology in UAV photogrammetry by using smartphone built-up system. In this research, the authors used Samsung Galaxy S, Galaxy S2 type A and type B attached on fixed-wing UAV with additional vibration-proof to do static and dynamic aerial

photogrammetry experiments with autofocus and infinity focus setting. The accuracy assessment of the built-in sensors in the static and dynamic experiments produced standard deviations of around 10 m for the location accuracy of the GPS. Also, the result showed that considering camera internal parameter in aerial triangulation process did not significantly improved the accuracy in dynamic experiment compared with the result of the static experiment.

(Rau, Jhan, and Li 2016) propossed stiching images with multicamera self-calibration method and analyze the internal accuracy of image, external absolute accuracy from bundle adjustment process and DSM data. The experimental result showed that an internal accuracy of image stiching is better than 1 pixel. For aerial triangulation, RMS of the control points and check points of the stitched images are less than 10 and 20 cm in horizontal and vertical directions. And lats, DSM data showed the consistency of level accuracy both in original and stiched images.

(Vallet et al. 2012) focused on the photogrammetric performance of an ultra light UAV equipped with a compact 12Mpix camera with online data processes provided by Pix4D software. The result then compared with the reference data from LiDAR-photogrammetric flight with Helimap System. The result showed that the quality of the mapping products issued from "Swinglet" UAV system seems to depend on the processing tools used. The quality of orthomosaic result from this system is not reaching the level of the reference flight.

2. METHODOLOGY

2.1. Research Design and Accuracy Assessment

The study area was conducted in NanGang Industrial Area, Nantou county, R.O.C (Taiwan) **(Figure. 1)**. The area size was approximately 1 km^2 that mostly covered by factory buildings and small portion of resident houses (located at south-east) and vegetation (located at north-west and separately cover the area between buildings).

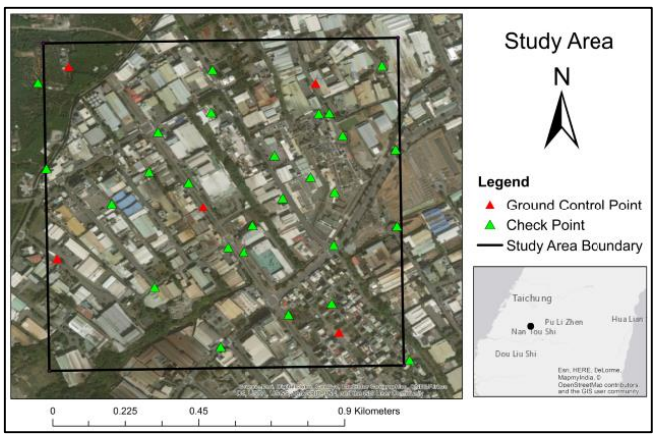

Figure 1. Overview of the Study Area Location. Black rectangular shape represents the study area boundary. Control points used in aerial triangulation process are represented in triangular shape. Red colour represents Ground Control Point while green colour represents Check Point location

To analyse the accuracy of UAV Photogrammetry measurement, then the authors designed the standard procedure as shown in **Figure.2**.

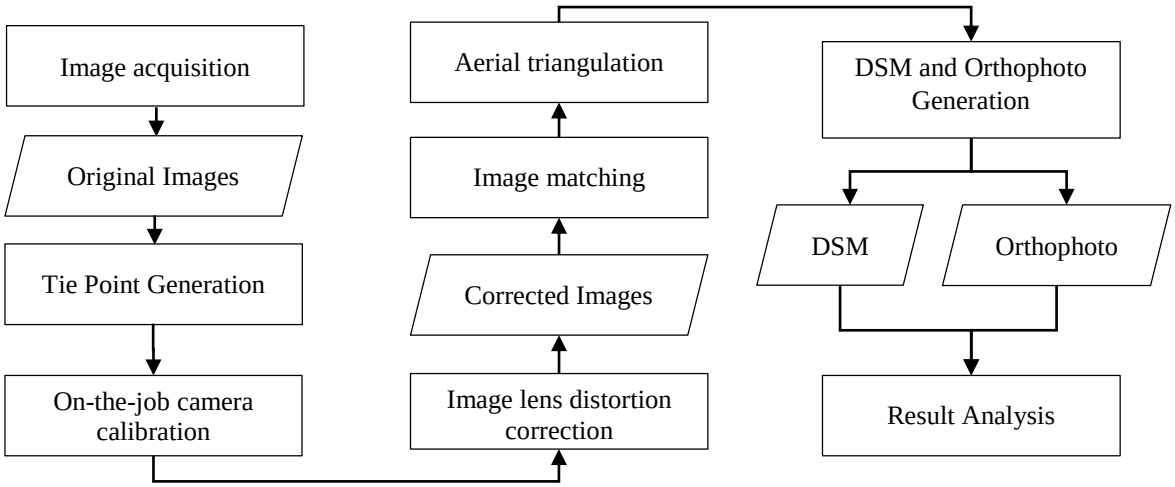

Figure 2. Research Standard Procedure

The general workflow was started from data acquisition which produced aerial images where the lens distortion still exist. Hereafter, these aerial images will be called as original images. Tie point from each dataset (dataset can be seen in **Table.**1) including merged data that generated from Pix4Dmapper software then were calibrated in Australis photometrix software. Internal camera parameter calculated from on-the-job calibration of Merged Data and Data 3 were used to remove lens distortion on corresponding original aerial images. Interior Orientation Parameter (IOP) from Merged Data was used to correct lens distortion on Data 4 to Data 9 while IOP from Data 3 was used to correct lens distortion on Data 1 to Data 3 aerial images. From this correction, we got the original images without lens distortion effect that hereafter these images were called as corrected images. Corrected images were processed in Pix4Dmapper software to perform image matching, aerial triangulation and DSM and orthophoto generation.

Accuracy assessment method was divided into three parts:

a. Camera Calibration
   Comparison of radial and decentering distortion value for each dataset including Merged Data from on-the-job calibration method was conducted to understand the lens distortion pattern of SODA camera before and after the firmware was updated. The authors also want to study the IOP result from indoor environment so that another test was set using the same type camera but different device. First is the camera from other device (has 1.1.0 firmware version) while second one is the camera used to take aerial images. Hereafter, first camera was named as SODA 1 and the second camera as SODA 2.
b. Aerial Triangulation
   In photogrammetry project, using control point only as traditional technic can improve the result accuracy while time and cost consumed for control point survey is one of critical issue. The presence of Real Time Kinematic (RTK) georeferencing technic with additional Post Processed Kinematic (PPK) correction can deliver accurate camera position and orientation which the result accuracy is comparable to traditional one. Based on this, the author assessed the aerial triangulation accuracy by comparing the used of different georeferencing method. The georeferencing cases presented here were used 5 GCPs only (GCP), RTK/PPK without using any GCP (RTK/PPK) and RTK/PPK together with 5 GCPs (RTK/PPK+5GCP). Root Mean Square Error (RMSE) of check points coordinate in horizontal and vertical direction was calculated to perform the accuracy analysis. Error was introduced by the coordinate differences between aerial triangulation result and original measurement data from GPS.
c. DSM and Orthophoto Generation
   RMSE of check points coordinate in horizontal and vertical direction digitized from DSM and orthophoto was calculated to perform the accuracy analysis. The term error here was introduced by the coordinate differences between DSM and orthophoto digitizing and original measurement data from GPS.

2.2 Instrumentation

eBee senseFly drone like shown in **Figure.3(a)** was used to acquire aerial images from 200, 400 and 600 m height. eBee senseFly is a wingspan drone model which only has 1.1 kg weight and can fly up to 59 minutes in one flight mission. To capture image, Sensor Optimized for Drone Application (S.O.D.A) camera as shown in **Figure.3(b)** was used. S.O.D.A camera is the first camera to be designed for professional drone photogrammetry produced by senseFly company. This camera has 20 Megapixel resolution, 2.4 micron of pixel size and 1-inch of sensor size. During the image acquisition period, the camera firmware was updated so that some of dataset were taken in different firmware version. In this research,

the author also used another camera (1.1.0 firmware version) with the same type but different device for additional camera calibration test.

(a) (b)

F**igure 3.** Research Instruments: (a)eBee senseFly Drone and (b)S.O.D.A senseFly Camera

Australis Photometrix software was used to process indoor and on-the-job camera calibration of aerial images tie point. Camera internal parameter calculated from Australis then was used to remove the lens distortion of original aerial images. Pix4Dmapper professional software version 3.1.22 was used to process aerial triangulation and generate DSM and orthophoto.

2.3 Research Material

Totally, 738, 204 and 128 geolocated aerial images corresponds to different flight height 200, 400, 600 m respectively were used (**Table.1**). For each flight height, aerial images were taken in double block (north-south and east-west blocks) which the percentage of overlap area between two images is 70% and between two strips is 60%. 5, 10 and 15 cm of Ground Sample Distance (GSD) can be achieved by flying the UAV at 200, 400 and 600 m height, respectively. Merged Data contains original aerial images of Data 6 and Data 9 that only used in camera calibration process.

In this research, 32 control points that constructed and measured using GPS geodetic by National Land Surveying and Mapping Center (NLSC), Ministry of Interior, R.O.C (Taiwan) were used to improve the aerial triangulation accuracy. The location of control point can be seen in **Figure.1**.

Table 1. Dataset Used

Description	**Data 1**	**Data 2**	**Data 3**	**Data 4**	**Data 5**	**Data 6**	**Data 7**	**Data 8**	**Data 9**	**Merged Data**
Camera Firmware	1.1.0			1.2.0						
Date taken	6/10/2017			6/25/2017						
Flight Altitude (m)	200			400			600			400 and 600
GSD (cm)	5			10			15			10 and 15
Total image	387	351	738	102	102	204	64	64	128	432
Block	North - South	East-West	Double Block	North-South	East-West	Double Block	North-South	East-West	Double Block	Double Block

2.4 Main Algorithm

2.4.1 Collinearity Equation

The observation equations which are the foundation of a bundle adjustment are the collinearity equations that denoted in Eq1. Collinearity equations represent the collinearity condition that the exposure station, any object point, and its photo image all lie along a straight line in three-dimensional space.

$$x_a = x_o - f\left[\frac{m_{11}(X_A - X_L) + m_{12}(Y_A - Y_L) + m_{13}(Z_A - Z_L)}{m_{31}(X_A - X_L) + m_{32}(Y_A - Y_L) + m_{33}(Z_A - Z_L)}\right]$$
$$y_a = y_o - f\left[\frac{m_{11}(X_A - X_L) + m_{12}(Y_A - Y_L) + m_{13}(Z_A - Z_L)}{m_{31}(X_A - X_L) + m_{32}(Y_A - Y_L) + m_{33}(Z_A - Z_L)}\right] \quad (1)$$

where
x_a and y_a = photo coordinates of image point a
X_A, Y_A and Z_A = object space coordinates of point A

X_L, Y_L and Z_L = object space coordinates of the exposure station
f = camera focal length
x_o and y_o = coordinates of the principal point
M = functions of three rotation angles, and most often omega, phi and kappa are the angles employed

2.4.2 Analytical Self Calibration

Is a computational process wherein camera calibration parameters are included in the photogrammetric solution, generally in a combined interior-relative-absolute orientation (Wolf and Dewitt 2000). Eq2 shows the analytical self-calibration equation.

$$x_a = x_o - \bar{x}_a(k_1 r_a^2 + k_2 r_a^4 + k_3 r_a^6) - (1 + p_3^2 r_a^2)[p_1(3\bar{x}_a^2 + \bar{y}_a^2) + 2p_2 \bar{x}_a y_a] - f\frac{r}{q}$$
$$y_a = y_o - \bar{y}_a(k_1 r_a^2 + k_2 r_a^4 + k_3 r_a^6) - (1 + p_3^2 r_a^2)[2p_1 \bar{x}_a y_a + p_2(\bar{x}_a^2 + 3\bar{y}_a^2)] - f\frac{s}{q} \quad (2)$$

where
x_a, y_a = measured photo coordinates related to fiducials
x_o, y_o = coordinates of the principal point
$\bar{x}_a$ = differences between image coordinate with principal point in x axis
$\bar{y}_a$ = differences between image coordinate with principal point in y axis
r_a^2 = summation and square of differences between image coordinate and principal point
k_1,k_2,k_3 = symmetric radial lens distortion coefficients
p_1,p_2,p_3 = decentering distortion coefficients
f = calibrated focal length
r,s,q = collinearity equation terms

3. RESULT AND DISCUSSION

The results were divided into three parts. First is camera calibration process. Second is aerial triangulation process and last is DSM and orthophoto generation process.

3.1 Camera Calibration

In aerial triangulation, camera internal parameter especially corresponds to lens distortion has high impact to object ground coordinate accuracy. Due to this issue, the authors want to remove lens distortion before aerial triangulation process by doing on-the-job calibration for all of dataset. IOP values used to remove lens distortion were chosen from Data 3 and Merged Data only based on its firmware version. Data 3 represented 1.1.0 firmware version while Merged Data represented 1.2.0 firmware version. Here, Data 6 and Data 9 were merged as one dataset named Merged Data, because the aerial images from those dataset were captured using camera with same firmware version (1.2.0 version). On this step, the authors added another calibration test from indoor environment of camera used to take aerial images and another camera with the same type but different device. IOP from indoor and on-the-job camera calibration of SODA 1, SODA 2, Data 3 and Merged Data were showed in **Table.2**. **Table.3** shows the summary of radial and decentering distortion of 1.1.0 and 1.2.0 firmware on the image sensor edge. The radial and decentering distortion curve of 1.1.0 and 1.2.0 firmware can be seen in **Figure.4**.

Table 2. IOP from Indoor and On-the-Job Calibration of SODA 1, SODA 2, Data 3 and Merged Data

Parameter	1.1.0 Firmware				1.2.0 Firmware			
	SODA 1 (Indoor Calibration)		Data 3 (On-the-Job Calibration)		SODA 2 (Indoor Calibration)		Merged Data (On-the-Job Calibration)	
	Value	Standard Error	Value	Standard Error	Value	Standard Error	Value	Standard Error
f (mm)	10.4957	< 0.001	10.5177	< 0.001	10.5817	< 0.001	10.5393	< 0.001
xp (mm)	-0.0025	< 0.001	-0.0791	< 0.001	-0.0851	< 0.001	-0.0807	< 0.001
yp (mm)	-0.0039	< 0.001	0.0179	< 0.001	0.0437	< 0.001	0.0112	< 0.001
K1	$-9.1*10^{-4}$	$1.1*10^{-19}$	$-1.0*10^{-3}$	$1.1*10^{-6}$	$9.9*10^{-4}$	$8.2*10^{-20}$	$8.2*10^{-4}$	$1.6*10^{-20}$
K2	$2.2*10^{-5}$	$1.1*10^{-23}$	$2.8*10^{-5}$	$5.0*10^{-8}$	$2.5*10^{-5}$	$8.2*10^{-24}$	$3.7*10^{-5}$	$1.6*10^{-24}$
K3	$-9.3*10^{-8}$	$1.1*10^{-29}$	$-1.9*10^{-7}$	$7.1*10^{-10}$	$-1.8*10^{-7}$	$8.2*10^{-30}$	$-3.8*10^{-7}$	$1.6*10^{-30}$
P1	$2.8*10^{-5}$	$1.1*10^{-19}$	$2.3*10^{-4}$	$5.5*10^{-7}$	$3.3*10^{-5}$	$8.2*10^{-20}$	$9.9*10^{-5}$	$1.6*10^{-20}$
P2	$-1.1*10^{-5}$	$1.1*10^{-19}$	$-1.1*10^{-4}$	$7.6*10^{-7}$	$-3.6*10^{-5}$	$8.2*10^{-20}$	$-1.1*10^{-4}$	$1.6*10^{-20}$

Table 3. Radial and Decentering Distortion Summary of 1.1.0 and 1.2.0 Firmware (Image Sensor Edge)

Lens Distortion	**Radial Distortion**				**Decentering Distortion**			
Camera Firmware	**1.1.0**		**1.2.0**		**1.1.0**		**1.2.0**	
Calibration	**Indoor**	**On-the-job**	**Indoor**	**On-the-job**	**Indoor**	**On-the-job**	**Indoor**	**On-the-job**
Min (pixel)	-	-18.04	-	193.46	-	5.65	-	1.83
Max (pixel)	-17.5	-20.96	197.5	197.13	0.79	6.19	0.88	2.73
Mean (pixel)	-	-19.74	-	195.4	-	5.96	-	2.42
Range (pixel)	-	2.92	-	3.67	-	0.54	-	0.90
Differences (pixel)	0.54 ~ 3.46		0.37 ~ 4.04		4.86 ~ 5.4		0.95 ~ 1.85	

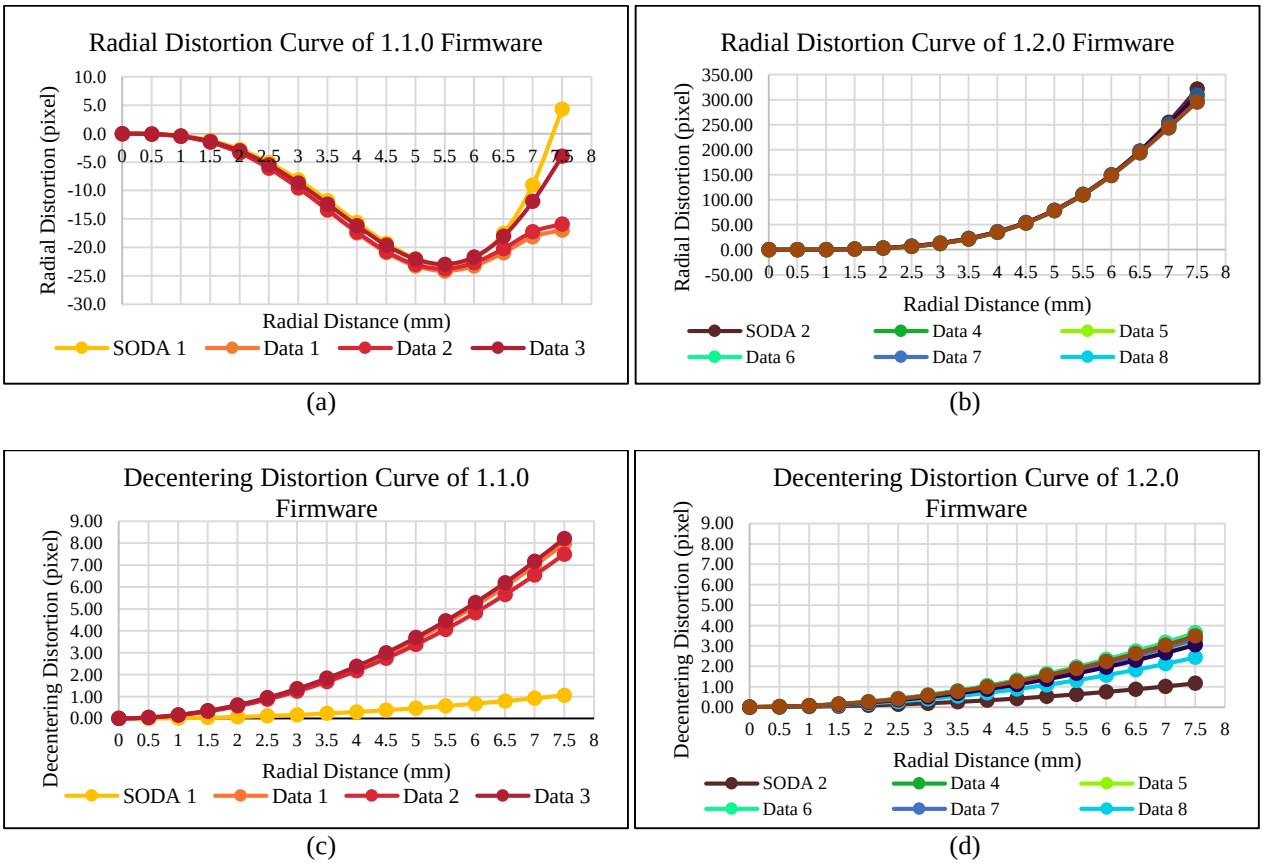

Figure 4. Lens Distortion Visualization: (a)Radial distortion of 1.1.0 firmware; (b)Radial distortion of 1.2.0 firmware; (c)Decentering distortion of 1.1.0 firmware and (d)Decentering distortion of 1.2.0 firmware

For camera calibration analysis, we focus on the radial distortion value at the edge of image sensor (6.5 cm of radial distance). **Table.3** shows the statistical record from radial and decentering distortion of all dataset including Merged Data. First, we look at radial distortion pattern for indoor and on-the-job calibration on 1.1.0 and 1.2.0 firmware version. We can see that radial distortion value of double block dataset from on-the-job calibration on 1.1.0 firmware (Data 3) is the lowest one (-18.04 pixel) compared to the single block dataset on same firmware (Data 1 and Data 2) which the range of maximum and minimum value is 2.92 pixel. Contrary, on 1.2.0 firmware we can see that radial distortion value of double block data set from on-the-job calibration (196.17 and 197.13 pixel for Data 6 and Data 9, respectively) is the highest one compared to single block dataset (Data 4, Data 5, Data 7 and Data 8) and Merged Data which the maximum minimum range is 3.67 pixel. According to this, taking aerial images in double block can assign bigger or smaller lens distortion effect even though not significantly than taking aerial images in single block. From the mean value, we can see that radial distortion of 1.2.0 firmware significantly increased around 175 pixel compared to 1.1.0 value from on-the-job calibration. This trend also can be seen on the maximum value from indoor calibration of both firmware which the differences is 180 pixel. This trend may indicate that the radial distortion effect has been obviously compensated by factory on previous firmware version (1.1.0) no matter what kind of environment was used to do camera calibration. If we look at the radial distortion value differences between indoor and on-the-job calibration for both 1.1.0 and 1.2.0 firmware version, no significance value was found since the differences value is only around 4 pixels. This satisfactory indicate that IOP from either indoor or on-the-job calibration can be used to remove lens distortion effect on aerial images.

Second, we look at decentering distortion pattern for indoor and on-the-job calibration. Different with radial distortion pattern, taking aerial images in double block at 1.1.0 firmware version (Data 3) can deliver highest decentering distortion value around 6.19 pixel which the minimum to maximum range is 0.54 pixel. Unclear pattern was occurred at 1.2.0 firmware while taking aerial images in double block may can provide same or lower decentering distortion value than taking aerial images in single block. Maximum value was delivered by Data 6 (2.73 pixel) while the range between maximum and minimum value is 0.9 pixel. Minimum to maximum decentering distortion range value for both firmware was less than 1 pixel. This shows that taking aerial images either in single or double block for both firmware versions can be made as an option since all of this technics do not give big impact to decentering distortion effect. Based on firmware, we can see that on-the-job calibration of 1.2.0 firmware has lower value around 3.54 pixel than 1.1.0 firmware while the value from indoor calibration showed similar for both firmware. This is not clear whether the decentering distortion effect has been compensated or not on previous firmware version since the value got from indoor environment looked similar while this is not be evidenced from on-the-job calibration result. Based on indoor and on-the-job calibration performance, we can see that there is no significance differences value between indoor and on-the-job calibration for both firmware since the value is around 5 pixel difference. This also satisfactory indicate that IOP from either indoor or on-the-job calibration can be used for removing lens distortion effect on aerial images or further process. Interested point was found on decentering distortion differences between indoor and on-the-job calibration of 1.1.0 firmware while value from on-the-job calibration is higher than indoor calibration. Further study and analysis is mandatory conducted to see the possible cause of systematic error from the flight data.

3.2 Aerial Triangulation

After IOP was calculated from Data 3 and Merged Data, lens distortion in original aerial images can be removed to get corrected images. Corrected images then were imported to Pix4Dmapper to do image matching, aerial triangulation and DSM and orthophoto generation processes. Previously mentioned that three different georeferencing technics were used and RMSE of check points coordinate were conducted. The RMSE of check point from aerial triangulation process using three different georeferencing technics can be seen in **Table.4**. Visualization of check point RMSE can be seen in **Figure.5**.

Table 4. Check Point RMSE from Aerial Triangulation

RMSE (m)	RTK/PPK+ 5GCP	5GCP	RTK/PPK	RTK/PPK+ 5GCP	5GCP	RTK/PPK	RTK/PPK+ 5GCP	5GCP	RTK/PPK
	North – South Block			**East – West Block**			**Double Block**		
	Data 1			**Data 2**			**Data 3**		
X	0.036	0.033	0.067	0.047	0.038	0.048	0.020	0.024	0.034
Y	0.038	0.027	0.095	0.066	0.027	0.097	0.026	0.017	0.080
XY	0.052	0.043	0.117	0.081	0.047	0.108	0.033	0.030	0.086
Z	0.066	0.194	0.288	0.130	0.201	0.371	0.069	0.179	0.353
	Data 4			**Data 5**			**Data 6**		
X	0.036	0.034	0.221	0.048	0.048	0.161	0.032	0.031	0.052
Y	0.061	0.055	0.133	0.073	0.043	0.135	0.051	0.038	0.095
XY	0.071	0.065	0.258	0.087	0.065	0.210	0.060	0.049	0.108
Z	0.109	0.111	1.713	0.153	0.098	1.721	0.095	0.089	1.741
	Data 7			**Data 8**			**Data 9**		
X	0.044	0.049	1.414	0.078	0.040	0.122	0.064	0.038	0.162
Y	0.032	0.036	1.320	0.057	0.030	0.233	0.029	0.025	0.225
XY	0.055	0.061	1.935	0.097	0.050	0.263	0.070	0.046	0.277
Z	0.167	0.061	3.496	0.158	0.169	2.691	0.076	0.113	2.841

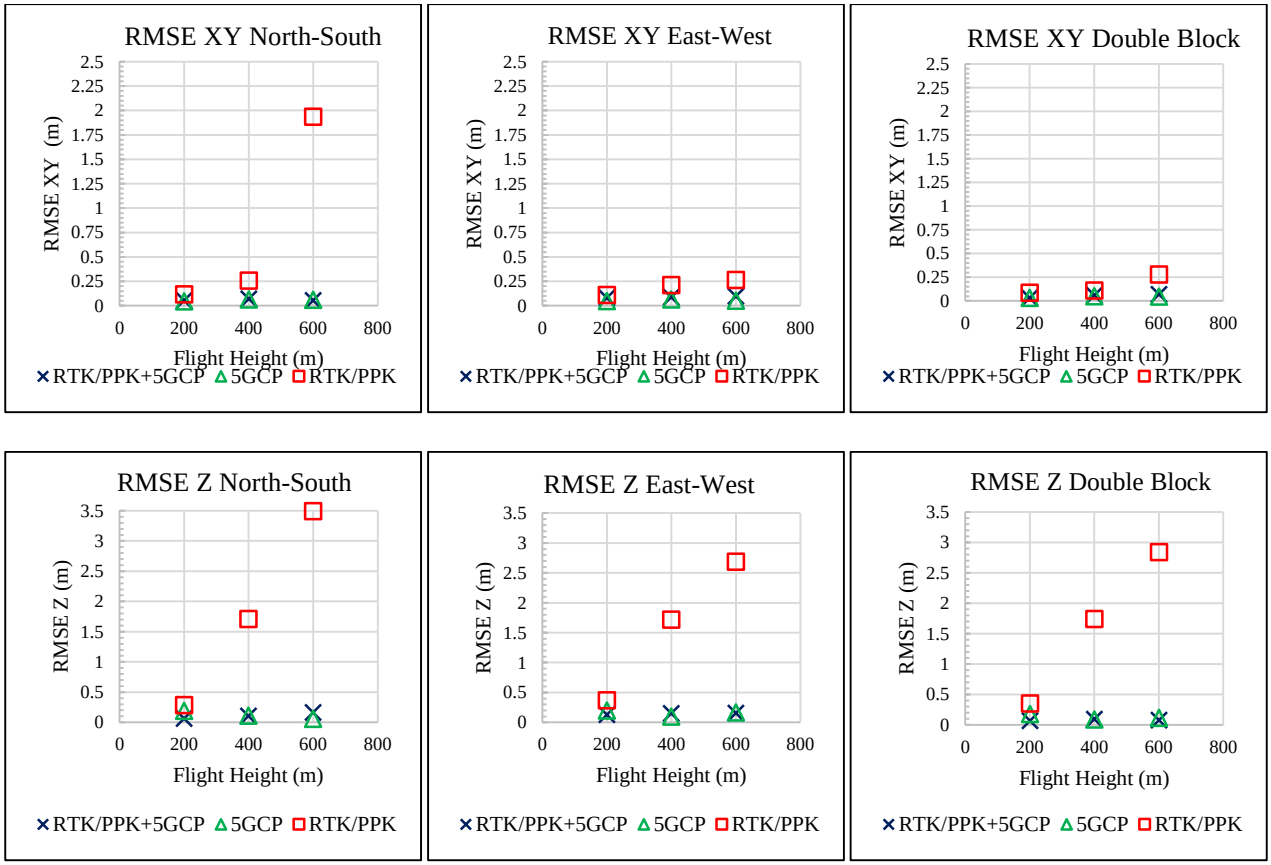

Figure 5. Visualization of Check Point RMSE for All Aataset Using Different Georeferencing Technique. Pictures above represent RMSE in horizontal direction while pictures below show RMSE in vertical direction

3.2.1 Georeferencing Technique Comparison

If we compare the RMSE value from those three georeferencing techniques, we can see that using RTK/PPK only gives the highest RMSE both in horizontal and vertical direction for all dataset either in single or double block. Maximum RMSE value was remarked on 2 m and 3 m in horizontal direction and vertical direction, respectively. This result is affected by RTK measurement performance. On this research, flight mission was conducted at urban area while obstruction such as building can interfere the communication link between central station and user (UAV). Low measurement accuracy can deliver inaccurate image position that affects the ground coordinate accuracy from aerial triangulation process. Inaccurate image position was represented by the high RMSE value from 600 m flight height dataset at north-south block which exceed to 2 m accuracy. RMSE value is more sensitive in vertical direction because positioning error in elevation of GNSS measurement is two times larger than in horizontal plan.

The ground coordinate accuracy can be improved either by using GCP only or combination of RTK/PPK and GCP. The used of GCP to control block deformation combined with RTK/PPK assisted image position was expected can provide best accuracy result. Same trend was explained in (Pix4Dmapper 2017) . While using GCP together with RTK georeferencing technique and post processed in PPK delivers better accuracy (0.048 m) than using RTK only (0.081 m) or RTK followed by PPK processing (0.067). Unexpected result was found where the best accuracy in horizontal direction was delivered by using GCP only, but not significantly varied while using RTK/PPK and GCP together in vertical direction. This issue may come from image position weighting while in this research, weight was set same as image position accuracy provided by UAV log file. Almost aerial images have good accuracy which the mean value is 2 cm and 4 cm in horizontal and vertical direction, respectively. Giving high weight when used RTK/PPK and GCP together can produce higher RMSE value. Further study about image position weighting impact to ground coordinate accuracy is mandatory conducted in the future.

3.2.2 Flight Height Impact Comparison

From the result above we can see that the trend of RMSE value both in horizontal and vertical direction will increase significantly by increasing of flight height when used RTK/PPK only. This trend also appeared when used either control point only (5GCP) or RTK/PPK combined with control point (RTK/PPK+5GCP) in horizontal direction while the

maximum difference value is around 3 cm. This finding was due to image overlap ratio between those three different flight height dataset. Increasing the flight height will reduce image overlap ratio so that affects image matching process and aerial triangulation performance. Different trend was found in vertical direction when used control point only (GCP). Both in single and double block, flying UAV at 400 m can deliver best accuracy while flying UAV at 200 m deliver worst accuracy.

3.2.3 Block Configuration Comparison

The last analysis was conducted to compare the influence of block configuration through ground coordinate accuracy. From the result above, we can see that flying UAV in double block can improve the accuracy both in horizontal and vertical direction for all georeferencing technique. Image overlap ratio is the factor to explain this finding. Image overlap ratio is higher when aerial images are taken in double block than taken in single block. When image overlap ratio was increased, more matched tie point will be generated and so that more object point can be calculated to perform better aerial triangulation process.

3.3 Orthophoto and DSM Generation

The final process was DSM and orthophoto generation. In this part, both DSM and orthophoto was generated in 15 cm resolution and the DSM grid spacing is 1 m. DSM and orthophoto generated from Data 3, Data 6 and Data 9 using RTK/PPK+5GCP georeferncing technique. Root mean square error between check points coordinate digitized from DSM and orthophoto through coordinate measured using GPS geodetic was conducted as accuracy assessment. **Table.5** shows the summary of check points RMSE from aerial triangulation and DSM and orthophoto generation process while its diagram comparison can be seen in **Figure.6**.

Table 5. Check Point RMSE from Aerial Triangulation and DSM and Orthophoto Generation Process

	Aerial Triangulation			DSM and Orthophoto		
RMSE (m)	**Data 3**	**Data 6**	**Data 9**	**Data 3**	**Data 6**	**Data 9**
X	0.020	0.032	0.064	0.079	0.067	0.083
Y	0.026	0.051	0.029	0.065	0.063	0.041
XY	0.033	0.060	0.070	0.102	0.092	0.092
Z	0.069	0.095	0.076	0.105	0.287	0.551

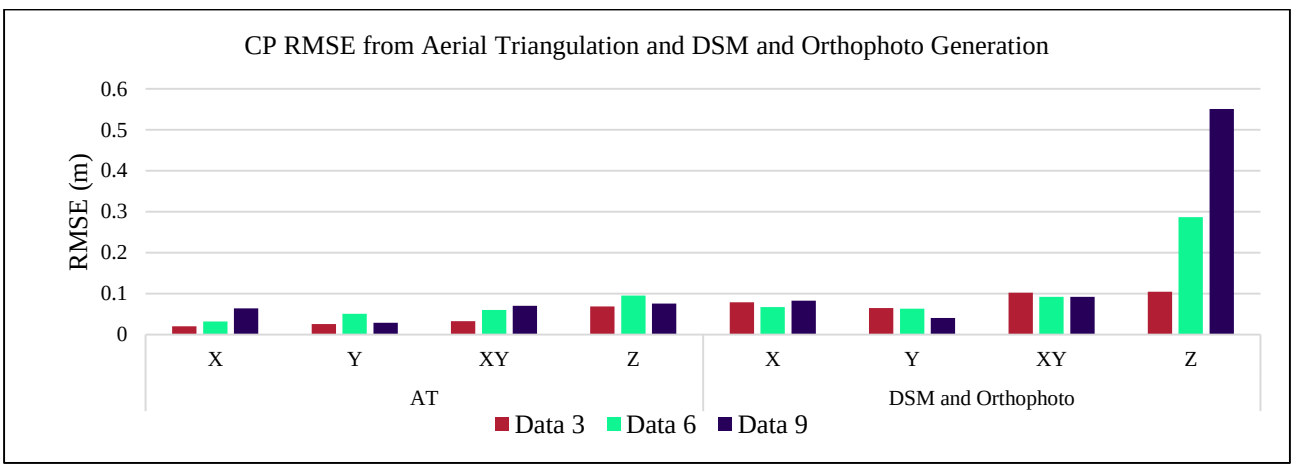

Figure 6. Diagram of Check Point RMSE from Aerial Triangulation and DSM and Orthophoto Generation

First we focus on RMSE value from DSM and orthophoto digitizing while the values are similar for three dataset in horizontal direction and increased by increasing of flight height in vertical direction. From the result above we can see that RMSE value both in horizontal and vertical direction from DSM and orthophoto digitizing process is higher than performed from aerial triangulation process. Significant difference was appeared in vertical direction of Data 9 while aerial images were taken from 600 m flight height. Since check points coordinate here was digitized from DSM and orthophoto, point accuracy was clearly affected by DSM and orthophoto raster visualization. Even though DSM and orthophoto were generated at same resolution for these three dataset, but it shows different visualization. The orthophoto

visualization at Data 3 is the best while Data 9 is the worst. This is affected by the fact that more tie points are detected in Data 3 than in either Data 6 or Data 9. By increasing of detected tie point, orthophoto visualization becomes better due to increasing of dense point cloud. Target point can be easily and more accurately marked on better orthophoto visualization. Because the diameter of target point center is 8 cm, then more accurate target point position can be achieved by digitizing orthophoto derived from 5cm GSD aerial images (Data 3). The other possible reason was come from dataset accuracy. DSM was generated from elevation interpolation while clearly affected by its accuracy. Because Data 9 delivers the highest elevation error from aerial triangulation process, then its DSM will deliver the highest elevation error.

4 CONCLUSION

Presented results showed the ground coordinate accuracy based on aerial triangulationa and DSM and orthophoto generation process. In aerial triangulation, analysis based on georeferencing techniques, flight height and block configuration comparisons were conducted. In urban area, using RTK/PPK georeferencing technique will deliver lowest accuracy compared with using GCP only and combination of RTK/PPK and GCP. Using GCP only can deliver best accuracy while image position weighting was a factor that should be studied when use RTK/PPK together with GCP. In horizontal direction, flying UAV at the lowest altitude (here is 200 m) and in double block can perform best accuracy for any georeferencing technique. Best accuracy in vertical direction can be delivered by flying UAV at the lowest altitude and used RTK/PPK+5GCP or RTK/PPK only. Even though, when used GCP only, flying UAV at the middle height (here is 400 m) can deliver best accuracy in vertical direction. Check point accuracy from DSM and orthophoto digitizing was worse than from aerial triangulation process where raster file visualization and each dataset accuracy were stated as the main factor. Since the DSM and orthophoto accuracy was influenced by aerial triangulation result, more careful experiment and analysis on aerial triangulation was mandatory conducted to see the possibility of using UAV photogrammetry as alternative measurement technique in the future.

5 REFERENCES

References from Journals:
Kim, Jinsoo, Seongkyu Lee, Hoyong Ahn, Dongju Seo, Soyoung Park, and Chuluong Choi. 2013. "Feasibility of Employing a Smartphone as the Payload in a Photogrammetric UAV System." *ISPRS Journal of Photogrammetry and Remote Sensing* 79. International Society for Photogrammetry and Remote Sensing, Inc. (ISPRS): 1–18. doi:10.1016/j.isprsjprs.2013.02.001.

Rau, Jiann Yeou, Jyun Ping Jhan, and Yi Tang Li. 2016. "Development of a Large-Format UAS Imaging System with the Construction of a One Sensor Geometry from a Multicamera Array." *IEEE Transactions on Geoscience and Remote Sensing* 54 (10): 5925–34. doi:10.1109/TGRS.2016.2575066.

References from Books:
Wolf, Paul R, and Bon A Dewitt. 2000. *Elements of Photogrammetry with Applications in GIS*. 3rded. USA: Mc Graw-Hill.

References from Other Literature:
Vallet, J., F. Panissod, C. Strecha, and M. Tracol. 2012. "Photogrammetric Performance of an Ultra Light Weight Swinglet 'Uav.'" *ISPRS - International Archives of the Photogrammetry, Remote Sensing and Spatial Information Sciences* XXXVIII-1/ (September): 253–58. doi:10.5194/isprsarchives-XXXVIII-1-C22-253-2011.

References from Websites:
Pix4Dmapper. 2017. "Do RTK/PPK Drones Give You Better Results than Using GCPs? - Pix4D." https://pix4d.com/rtk-ppk-drones-gcp-comparison/.